Self-assembly in aqueous solution of wheel-shaped Mo_{154} oxide clusters into vesicles

Tianbo Liu[1], Ekkehard Diemann[3], Huilin Li[2], Andreas W. M. Dress[4] & Achim Müller[3]

[1]*Department of Physics,* [2]*Department of Biology, Brookhaven National Laboratory, Upton, New York 11973, USA*
[3]*Faculty of Chemistry,* [4]*Faculty of Mathematics, University of Bielefeld, D-33501 Bielefeld, Germany*

Surfactants and membrane lipids readily assemble into complex structures[1] such as micelles, liposomes or hollow vesicles owing to their amphiphilic character—the fact that part of their structure is attracted to polar environments while another part is attracted to non-polar environments. The self-assembly of complex structures also occurs in polyoxometallate chemistry, as exemplified by the molybdenum blue solutions known for centuries. But while the presence of nanometre-sized metal oxide aggregates in these solutions has long been recognized, unravelling the composition and formation process of these aggregates proved difficult. Recent work has indicated that discrete, wheel-shaped mixed-valence polyoxomolybdate clusters of the type {Mo_{154}} (refs 2–4) assemble into well-defined nanometre-sized aggregates, including spherical structures[5]. Here we report light-scattering data and transmission electron microscopy images of hollow spherical structures with an average, almost monodisperse radius of about 45 nm and composed of approximately 1,165 {Mo_{154}} wheel-shaped clusters. The clusters appear to lie flat and homogeneously distributed on the vesicle surface. Unlike conventional lipid vesicles, the structures we observe are not stabilized by hydrophobic interactions. Instead, we believe the polyoxomolybdate-based vesicles form owing to a subtle interplay between short-range van der Waals attraction and long-range electrostatic repulsion, with important further stabilization arising from hydrogen bonding involving water molecules encapsulated between the wheel-shaped clusters and in the vesicles' interior.

Centuries ago, Native Americans observed a mysterious "blue water", which is now thought to have been the molybdenum blue solution formed naturally upon oxidation of molybdenite, MoS_2 (ref. 4). The presence of nanometre-sized metal oxide aggregates in solution can easily be proved by the Tyndall effect and trying to unravel the exact composition and structure of the dissolved entities has long been a challenging problem, attracting the interest of chemists such as Scheele[6] and Berzelius[7]. But firm insights into the complex molecular structure of the anionic units have emerged only over the last decade, following controlled synthesis and subsequent precipitation of giant wheel-shaped {Mo_{154}} anions[4] derived from molybdenum blue (see Fig. 1a–c). Because these anions have highly hydrophilic surfaces that render them extremely soluble, they are preferably precipitated under high concentration or through a salting-out process[2–4,8], analogous to the salting-out of proteins. The giant wheel-shaped anions have a composition almost identical to that of natural molybdenum blue (the mineral ilsemannite, approximate formula $Mo_3O_8{\cdot}nH_2O$)[9]. A preliminary study indicated that they aggregate into large spherical assemblies that burst in vacuum[5], suggesting a hollow, vesicle-like aggregate structure.

To further elucidate the composition and structure of the aggregates, we performed static and dynamic light scattering (SLS and DLS) measurements a few days after their aggregation and growth in water was complete. The parent solution was prepared using the well-defined crystalline product $Na_{15}[Mo(VI)_{126}Mo(V)_{28}O_{462}H_{14}(H_2O)_{70}]_{0.5}[Mo(VI)_{124}Mo(V)_{28}O_{457}H_{14}(H_2O)_{68}]_{0.5}\cdot\sim 400\ H_2O$, which contains, beside Na^+ and H^+ ions, {Mo_{154}}- and {Mo_{152}}-type anionic units (the latter unit has properties identical to those of the former, and is missing only one Mo_2 unit)[2–4]. The results of a CONTIN analysis[10] of DLS measurement performed on the aqueous {Mo_{154}} solution are shown in the inset of Fig. 2, demonstrating that the aggregates have an almost monodisperse size, with an average hydrodynamic radius R_h of ~45 nm. SLS data, analysed through the Zimm plot[11], indicate that the average radius of gyration R_g of the aggregates is 45.2 ± 1.4 nm (Fig. 2), that is, the two radii are identical. For a solid spherical particle, the relationship between the radii is $R_g = 0.77R_h$. If our aggregates were solid spheres with $R_h = 45$ nm, we would expect an R_g value of ~34 nm, which is clearly not the case. As an increasing fraction of the total mass of a spherical object is distributed closer to the sphere's surface, the ratio R_g/R_h increases; the ratio approaches a value of 1 as the corresponding spherical object has all its mass on its surface, the typical model for a vesicle structure[12]. Our scattering data thus indicate that the aggregates in solution are not 'solid clusters', but vesicle-like hollow spheres.

The mass of the aggregates (M_w) determined from the Zimm plot is $\sim(2.54 \pm 0.25) \times 10^7\ g\,mol^{-1}$, which corresponds to ~1,165 individual nanowheels. Because a solid {Mo_{154}}/{Mo_{152}}-type nanocrystal with a 45-nm radius would contain more than 14,000 individual molecules, the estimated M_w value also suggests that our aggregates must have a hollow interior. As a model (see

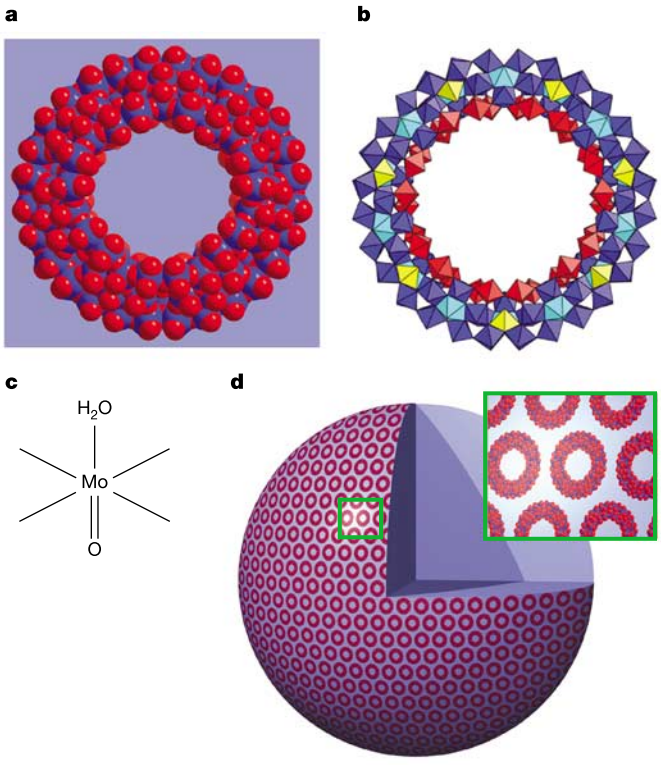

Figure 1 Structure of the 3.6 mm size {Mo_{154}}-type nanowheel with a hydrophilic surface and nanosized central cavity. **a**, Space-filling representation (blue and light blue, Mo atoms; red, O atoms). **b**, Polyhedral representation, demonstrating the abundance of pentagonal (Mo)Mo_5 units (in blue) probably influencing the water structure (Mo_2 units in red, Mo_1 units in yellow). **c**, The typical smallest fragment with a metal atom and its coordination sphere, that is, with one of the 70 H_2O ligands causing the extreme hydrophilic nature that is responsible for the interaction with solvents such as water. **d**, Schematic plot of the vesicle structure formed from nanowheels (~45 nm radius) in aqueous solution, with inset showing enlarged nanowheels.

illustration in Fig. 1d), we suggest that ~1,165 nanowheels are homogeneously distributed on the surface of a vesicle, with their molecular isotropic *x*–*y* plane parallel to the surface. If the *x*–*y* plane were perpendicular to the vesicle surface, the nanowheels would be expected to exhibit tubular rather than spherical morphology. In fact, a tubular morphology has been reported for the liquid crystal structure obtained from the present nanowheels encapsulated in surfactants[13].

Assuming that all the nanowheels are distributed on the surface by almost hexagonal closest packing, the centre-to-centre distance between two adjacent nanowheels would be $\sim 4.9 \pm 0.4$ nm, whereas the diameter of an individual nanowheel is ~3.6 nm[2]. This suggests that the nanowheels are not touching each other on the vesicle surface, and that water plays an important role in filling gaps and holding the overall assemblies together. Note that all the water molecules incorporated into the vesicle structures do not contribute to the scattered intensity ($dn/dc = 0$); the M_w value we have estimated from the scattering data does thus not include the weight of any water molecules incorporated into the vesicle. We estimate that if the weight of the water molecules were to be included, the actual M_w of the vesicles would be more than ten times larger than quoted above.

Placing our solution on a support and drying it allowed for high-resolution TEM studies, which indicate the presence of uniform, spherical entities of 35–45 nm in radius, corresponding to the abundance of the vesicles (Fig. 3a). The size range is consistent with the DLS and scanning electron microscope (SEM) measurements. The vesicles tend to burst and collapse during the drying process and hence to lose much water, with the result that the metal-oxide components are closer to each other in the burst product. We occasionally found larger vesicles and chose one of these for a more detailed study that yields better images (Fig. 3b). The burst ('post mortem') vesicle exhibits the wrinkle feature and high contrast around the edge typical for an empty sphere, as seen in case of the lipid vesicles; this observation is suggestive of the soft and flexible nature of the 'surface membrane' of our vesicles. When studying a patch of a broken vesicle flattened on the support carbon film (Fig. 3c), we observed locally ordered packing over small areas but no long-range order, as expected (Fig. 3d, e). Power diffraction spectra taken on these samples clearly indicate some ordering with lattice spacings of 4.2, 4.2 and 3.6 nm, respectively (Fig. 3f, g). Fourier filtering yields the images (Fig. 3h, i) while the real space distance ~3.6 nm corresponds exactly to the wheel diameter, which indicates that the wheels are in direct non-covalent contact after the vesicle has burst following loss of water in the high-vacuum condition.

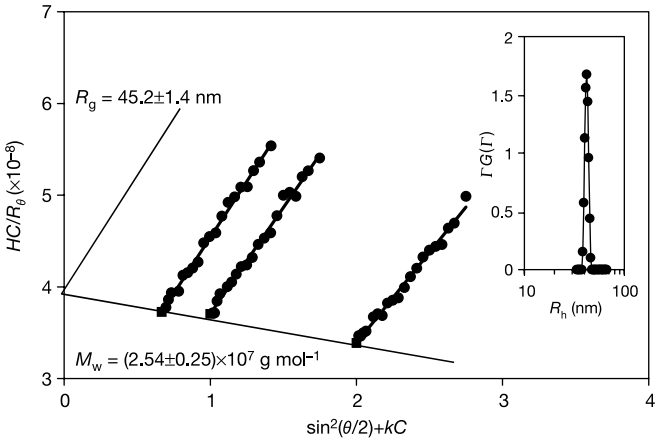

Figure 2 Zimm plot based on SLS measurements. Three different concentrations (from right, 0.03, 0.015 and 0.01 mg ml^{-1}, respectively, at pH = 2.3) are measured. The R_g and the weight-average mass of the aggregates (M_w) can be calculated from the plot (*H*: an optical parameter; *C*: vesicle concentration; R_θ: Rayleigh ratio of vesicle solution at scattering angle θ). Inset, CONTIN analysis of DLS study on 0.01 mg ml^{-1} {Mo_{154}}/{Mo_{152}} aqueous solution at pH = 2.3, scattering angle = 60°. The aggregates in solution have an average R_h of 45 nm, with a very narrow size distribution.

In contrast to surfactant vesicles assembled by hydrophobic interactions, the present vesicles consist of components that do not have any obvious hydrophobic parts and also keep a considerable distance from each other in the aggregate. We believe that the driving force for the assembly of these structures is a delicate balance between short-range attractive forces (van der Waals forces and hydrogen-bonding forces) and repulsive electrostatic interactions between adjacent anion clusters. This view is supported by the fact that vesicle size can be tuned by adjusting the pH of the solution or adding electrolytes, with larger vesicles ($R_h > 100$ nm) observed at lower pH conditions or in the presence of additional electrolyte such as NaCl. Considering that van der Waals interactions are relatively weak, additional stabilizing interactions are probably needed to keep the system together. This might be provided by hydrogen bonding involving (probably partly protonated) water molecules incorporated in the vesicle structures.

When structures are formed through the assembly of identical constituents, those exhibiting the highest symmetry tend to be energetically preferred[14,15]; thus, if surfaces of the present type are formed, highly symmetrical spherical structures might be expected. In the case of the {Mo_{154}} nanowheels arranged on a sphere, symmetry considerations suggest that the triangular net obtained by connecting the centres of any two adjacent nanowheels by a straight line should be an icosadeltahedron, that is, a polytope with icosahedral symmetry where all faces are equilateral triangles and either six or five triangles are found adjacent to each vertex. Icosadeltahedra were first classified by Goldberg and are parameterized by two integers, *h* and *k*, that describe the mutual position of centres of five-fold symmetry within the triangular net relative to each other. Defining the triangulation number[16] by $t = h^2 + hk + k^2$, the icosadeltahedron with parameters *h*,*k* has exactly $20t$ triangular faces and $2 + 10t$ vertices; 12 of these vertices are adjacent to five triangles and all other vertices are adjacent to six triangles. Consequently, vesicles can be expected to contain $2 + 10t$ wheels for some *h*,*k* values with $2 + 10t$ close to 1,165, the number obtained from our measurements. The condition $1{,}115 < 2 + 10t < 1{,}215$ holds only for $\{h,k\} = \{8,4\}$, and $\{9,3\}$, suggesting a corresponding number of $1{,}122 = 2 + 10(8^2 + 8\times4 + 4^2)$, or $1{,}172 = 2 + 10(9^2 + 9\times3 + 3^2)$ wheels within a vesicle.

Both SEM[5] and DLS measurements show that when using solvents with lower polarity, larger spherical aggregates form. For example, in acetone, uniform spherical vesicles with $R_h \approx 130 \pm 5$ nm and $R_g \approx 128.1 \pm 5.6$ nm are observed. Each vesicle contains ~19,000 single components, corresponding to a ~3.6 nm centre-to-centre distance, nearly the same as their actual size in single crystals[2]. This suggests that the nanowheels pack rather closely with each other to form a spherical shell in acetone. Their behaviour is in accord with the expectation that, as would any electrolyte, the anionic nanowheels should carry a lower charge in a weaker polar solvent (with cations expected to be correspondingly abundant at the anions' surface), leading to weaker inter-nanowheel repulsive electrostatic interactions, and thus to a smaller inter-nanowheel distance.

Further study is required to gain full insight into the unusual solution behaviour of the nanowheels and understand the nature of the interactions that drive the assembly in dilute solution against entropic effects. But we expect nevertheless that this unusual system will offer intriguing possibilities for further exploration and modification[4,13,17–20], given the structural complexity of the nanowheel building blocks, their extended hydrophilic surface, unusual geo-

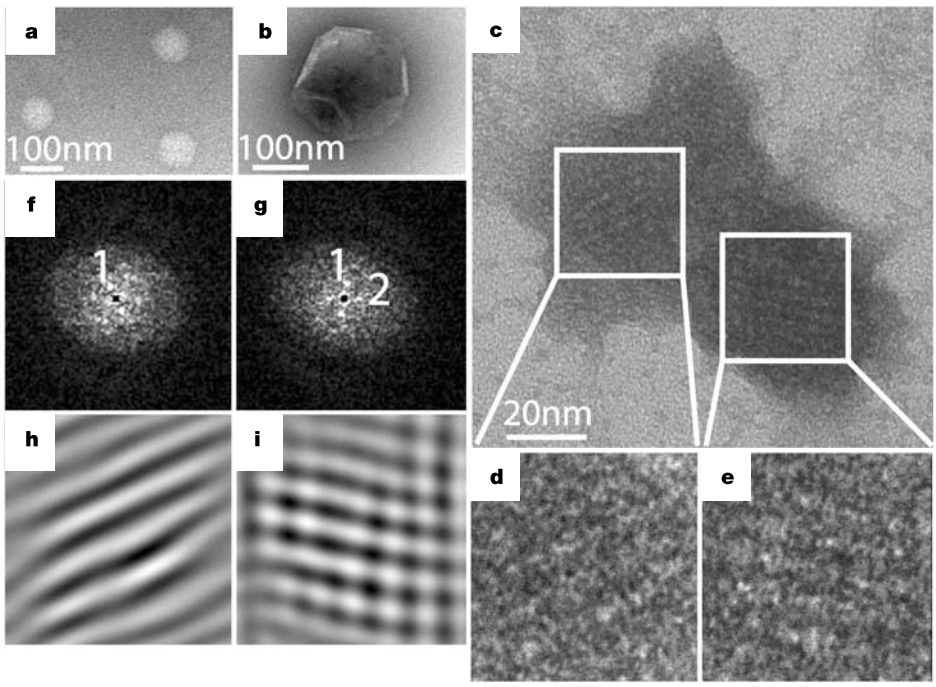

Figure 3 Transmission electron microscopy studies of wheel-type vesicles on carbon film. **a**, 35–45 nm radius vesicles; **b**, image of a larger broken vesicle; **c**, image of a small patch of the broken vesicle flattened on the support carbon film. **d**–**i**, Sub-areas, demarcated by two square boxes, are zoomed into (**d**, **e**). **f**, **g**, The corresponding Fourier transforms (power spectra) which clearly show some ordered packing in small local areas (one in **f** and two in **g**). **h**, **i**, Their back-transforms after filtering the high frequencies, showing the ordering of the nanowheels (diameter, 3.6 nm).

metrical structure and large number of delocalized electrons (causing the blue colour)[4].

Note added in proof: Until immediately before publication, we failed to cite two earlier papers of ours[21,22] that reported the vesicle formation behaviour of another polyoxometallate system. □

Methods

Static light scattering

A commercial Brookhaven Instrument LLS spectrometer equipped with a solid-state laser operating at 532 nm was used for measurements of both SLS and DLS. SLS experiments were performed at scattering angles between 10 and 120°, at 2° intervals. The basis of the SLS data analysis is the Rayleigh–Gans–Debye equation[11] to obtain the radius of gyration (R_g) and the weight-average molar mass (M_w) of the particles. As the present solutions indicate a certain absorption of the incident laser beam, the adsorption coefficients were measured by using an ultraviolet–visual (UV/vis) spectrophotometer at 532 nm to correct the incident and scattered laser strength. The fact that wheel-shaped anions were slowly oxidized helped to reduce the disturbing absorption (see below). The LLS measurement shows correspondingly that the scattered intensity continuously decreases owing to vesicle destruction. The smaller molybdates(VI), being decomposition products, do not contribute much to the scattered intensity. Only the final vesicles with the correct number of Mo(V) centres give the light-scattering signals observed. UV/vis spectrometry was used to determine the final nanowheel concentration based on the known extinction coefficient. The same supramolecular structures are of course also observed under exclusion of O_2, that is, in dark blue solutions.

Dynamic light scattering

DLS measures the intensity–intensity time correlation function by means of a BI-9000AT multi-channel digital correlator. The field correlation function $|g^{(1)}(\tau)|$ was analysed by the constrained regularized CONTIN method[10], to yield information on the distribution of the characteristic linewidth Γ from $|g^{(1)}(\tau)| = \int G(\Gamma)e^{-\Gamma\tau}d\Gamma$. The normalized distribution function of the characteristic linewidth, $G(\Gamma)$, so obtained, can be used to determine an average apparent translational diffusion coefficient, $D_{app} = \Gamma/q^2$. The hydrodynamic radius R_h is related to D via the Stokes–Einstein equation: $R_h = kT/(6\pi\eta D)$ where k is the Boltzmann constant and η the viscosity of the solvent at temperature T. From DLS measurements, we can obtain the particle-size distribution in solution from a plot of $\Gamma G(\Gamma)$ versus R_h. The R_h of the particles is obtained by extrapolating $R_{h,app.}$ to zero solute concentration and zero scattering angle. The R_h value of the $\{Mo_{154}\}/\{Mo_{152}\}$ vesicles does not show any obvious angular dependence, suggesting a spherical nature of the aggregates.

Transmission electron microscopy

Samples were prepared by pipetting 5 μl of solution onto a freshly glow discharged carbon-coated electron microscopy grid, and after blotting excess liquid, 5 μl of 2% uranyl acetate aqueous solution was used to negatively stain the sample. The negative-stain method provides better sample contrast while keeping the structural details to around 1 nm resolution. Microscopy observation was performed in a Jeol JEM-1200EX microscope. Images were recorded on Kodak SO-163 films and developed with standard procedure. Negative films were digitized with a Nikon Super Coolscan 8000 scanner. The image-processing software SPIDER http://www.wadsworth.org/spider_doc/spider/docs/master.html was used to generate the power spectra.

Received 17 February; accepted 2 September 2003; doi:10.1038/nature02036.

1. Evans, D. F. & Wennerström, H. *The Colloidal Domain: Where Physics, Chemistry, Biology, and Technology Meet* 2nd edn (Wiley, Chichester, 1999).
2. Müller, A. *et al.* Rapid and simple isolation of the crystalline molybdenum-blue compounds with discrete and linked nanosized ring-shaped anions: $Na_{15}[Mo^{VI}_{126}Mo^{V}_{28}O_{462}H_{14}(H_2O)_{70}]_{0.5}[Mo^{VI}_{124}Mo^{V}_{28}O_{457}H_{14}(H_2O)_{68}]_{0.5}\cdot ca.400H_2O$ and $Na_{22}[Mo^{VI}_{118}Mo^{V}_{28}O_{442}H_{14}(H_2O)_{58}]\cdot ca.250H_2O$. *Z. Anorg. Allg. Chem* **625,** 1187–1192 (1999).
3. Cronin, L., Diemann, E. & Müller, A. in *Inorganic Experiments* 2nd edn (ed. Woollins, J. D.) 340–346 (Wiley-VCH, Weinheim, 2003).
4. Müller, A. & Serain, C. Soluble molybdenum blues—"des Pudels Kern". *Acc. Chem. Res.* **33,** 2–10 (2000).
5. Müller, A. *et al.* Hierarchic patterning: architectures far beyond "giant molecular wheels". *Chem. Commun.* 1928–1929 (2001).
6. Scheele, C. W. in *Sämtliche Physische und Chemische Werke* (ed. Hermbstädt, D. S. F.) Vol. 1, 185–200 (Martin Sändig oHG, Niederwalluf/Wiesbaden, 1971) [reprint from 1793 original].
7. Berzelius, J. J. Beitrag zur näheren Kenntniss des Molybdäns. *Poggend. Ann. Phys. Chem.* **6,** 369–392 (1826).
8. Müller, A., Kögerler, P. & Kuhlmann, C. A variety of combinatorially linkable units as disposition: from a giant icosahedral Keplerate to multi-functional metal-oxide based network structures. *Chem. Commun.* 1347–1358 (1999).
9. Rösler, H. J. *Lehrbuch der Mineralogie* 418 (Deutscher Verlag für Grundstoffindustrie, Leipzig, 1991).
10. Provencher, S. W. CONTIN: A general purpose constrained regularization program for inverting noisy linear algebraic and integral equations. *Comput. Phys. Commun.* **27,** 229–242 (1982).
11. Hiemenz, P. C. & Rajagopalan, R. *Principles of Colloid and Surface Chemistry* Ch. 5 (Marcel Dekker, New York, 1997).
12. Zhou, S. *et al.* Spherical bilayer vesicles of fullerene-based surfactants in water: a laser light scattering study. *Science* **291,** 1944–1947 (2001).
13. Polarz, S., Smarsly, B. & Antonietti, M. Colloidal organization and clusters: self-assembly of polyoxometalate-surfactant complexes towards three-dimensional organized structures. *ChemPhysChem* **2,** 457–461 (2001).
14. Müller, A. *et al.* Generation of cluster capsules (I_h) from decomposition products of a smaller cluster (Keggin - T_d) while surviving ones get encapsulated: species with core-shell topology formed by a fundamental symmetry-driven reaction. *Chem. Commun.* 657–658 (2001).
15. Müller, A. The beauty of symmetry. *Science* **300,** 749–750 (2003).
16. Caspar, D. & Klug, A. Physical principles in construction of regular viruses. *Cold Spring Harb. Symp. Quant. Biol.* **27,** 1–24 (1962).

17. Kurth, D. G., Volkmer, D., Ruttorf, M., Richter, B. & Müller, A. Ultrathin composite films incorporating the nanoporous isopolyoxomolybdate "Keplerate" $(NH_4)_{42}[Mo_{132}O_{372}(CH_3COO)_{30}(H_2O)_{72}]$. *Chem. Mater.* **12,** 2829–2831 (2000).
18. Polarz, S., Smarsly, B., Göltner, C. & Antonietti, M. The interplay of colloidal organization and oxo-cluster chemistry: polyoxometalate-silica hybrids—materials with a nanochemical function. *Adv. Mater.* **12,** 1503–1507 (2000).
19. Müller, A., Shah, S. Q. N., Bögge, H. & Schmidtmann, M. Molecular growth from a Mo_{176} to a Mo_{248} cluster. *Nature* **397,** 48–50 (1999).
20. Müller, A., Toma, L., Bögge, H., Schmidtmann, M. & Kögerler, P. Synergetic activation of "silent receptor" sites leading to a new type of inclusion complex: integration of a 64-membered ring comprising K^+ and SO_4^{2-} ions into a molybdenum oxide-based nanoobject. *Chem. Commun.* 2000–2001 (2003).
21. Liu, T. B. Supramolecular structures of polyoxomolybdate-based giant molecules in aqueous solution. *J. Am. Chem. Soc.* **124,** 10942–10943 (2002).
22. Liu, T. B. An unusually slow self-assembly of inorganic ions in dilute aqueous solution. *J. Am. Chem. Soc.* **125,** 312–313 (2003).

Acknowledgements We thank M. Schmidtmann for the generation of Fig. 1d. T.L. acknowledges support of this work by the US Department of Energy, Division of Materials Science, and A.M. correspondingly, the Deutsche Forschungsgemeinschaft, the European Union, the Fonds der Chemischen Industrie, and the Volkswagen-Stiftung. H.L. acknowledges the support of the LDRD fund from BNL.

Competing interests statement The authors declare that they have no competing financial interests.

Correspondence and requests for materials should be addressed to T.L. (liu@bnl.gov) or A.M. (a.mueller@uni-bielefeld.de).

Interaction of sea water and lava during submarine eruptions at mid-ocean ridges

Michael R. Perfit[1], Johnson R. Cann[2], Daniel J. Fornari[3], Jennifer Engels[4], Deborah K. Smith[3], W. Ian Ridley[6] & Margo H. Edwards[5]

[1]*Department of Geological Sciences, University of Florida, Gainesville, Florida 32611, USA*
[2]*Department of Earth Sciences, University of Leeds, Leeds LS2 9JT, UK*
[3]*Woods Hole Oceanographic Institution, Geology and Geophysics Department, Woods Hole, Massachusetts 02543, USA*
[4]*Department of Geology and Geophysics,* [5]*Hawaii Institute of Geophysics and Planetology, School of Ocean and Earth Science and Technology, University of Hawaii at Manoa, Honolulu, Hawaii 96822, USA*
[6]*US Geological Survey, Mineral Resources Team, Denver, Colorado 80225, USA*

Lava erupts into cold sea water on the ocean floor at mid-ocean ridges (at depths of 2,500 m and greater), and the resulting flows make up the upper part of the global oceanic crust[1]. Interactions between heated sea water and molten basaltic lava could exert significant control on the dynamics of lava flows and on their chemistry. But it has been thought that heating sea water at pressures of several hundred bars cannot produce significant amounts of vapour[2–5] and that a thick crust of chilled glass on the exterior of lava flows minimizes the interaction of lava with sea water. Here we present evidence to the contrary, and show that bubbles of vaporized sea water often rise through the base of lava flows and collect beneath the chilled upper crust. These bubbles of steam at magmatic temperatures may interact both chemically and physically with flowing lava, which could influence our understanding of deep-sea volcanic processes and oceanic crustal construction more generally[6]. We infer that vapour formation plays an important role in creating the collapse features that characterize much of the upper oceanic crust and may accordingly contribute to the measured low seismic velocities in this layer.

Lobate and sheet lava flows erupted at axes of intermediate- and fast-spreading mid-ocean ridges (MORs) can extend for kilometres from their eruptive fissures as uppermost (~0–500 m) oceanic crust is constructed[1]. MOR lava flows commonly contain depressions where thin crusts, 2–10 cm thick, forming flow surfaces, have collapsed into cavities beneath (see, for example, refs 6–11). Tabular pieces of lava crust often accumulate on the floor of the depressions; alternatively, the roof of the flow may remain in place, supported by lava pillars (Fig. 1a). The common occurrence of lava pillars in this setting is explained by the passage of large volumes of heated sea water up through an advancing and inflating lava flow or pond[12–15].

Sea-floor lava crusts have 1–2-cm-thick glassy margins on their exterior surfaces formed during the quenching of molten lava by cold (~2–4 °C) sea water, but frequently have thinner, partly glassy margins on their underside surface. Delicate drip structures and a variety of other surface morphologies are commonly observed on the underside of crusts, but not on the exterior surfaces. The features include: (1) mesocrystalline to glassy rinds a few milli-

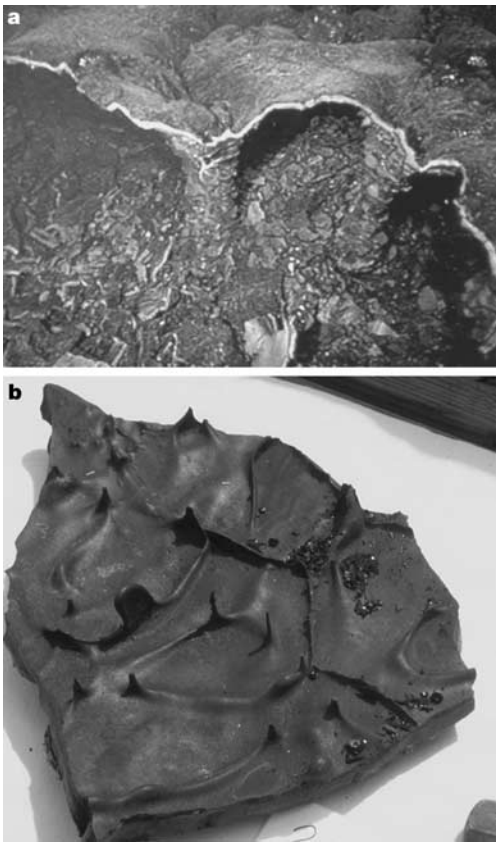

Figure 1 Macroscopic features of mid-ocean-ridge basalts indicative of magma–sea water interaction. **a**, Side-view into a deep-sea lobate lava flow on the East Pacific Rise crest near 9° 50′ N at 2,510 m depth. Two lava pillars in the central portion of the photograph are supporting the bowed-up upper crust of the flow that is ~4–10 cm thick. Distance between flow surface and the floor is ~1 m. Platy talus from collapse of portions of the lava crust cover the sea floor in the foreground. Width across photograph taken from the submersible *Alvin* is ~4 m. (Photograph courtesy of Woods Hole Oceanographic Institution, Deep Submergence Operations Group.) **b**, Interior of a deep-sea lobate lava crust (concave side that faces down) from the East Pacific Rise crest at 2,510 m depth showing delicate drip structures and well-developed septa that separate areas where bubbles and cavities of briny vapour at magmatic temperature existed during formation of the drips. Width across photograph is 20 cm, individual drips are ~2–4 cm long. Although the surface appears to be smooth and glassy, optical microscopy and SEM images (see Figs 2 and 3) show a variety of textures and minerals comprise these surfaces.

